John von Neumann Institute for Computing

Exact Diagonalization Results for Strongly Correlated Electron-Phonon Systems

Holger Fehske, Alexander Weiße, Gerhard Wellein

published in

NIC Symposium 2001, Proceedings,
Horst Rollnik, Dietrich Wolf (Editors),
John von Neumann Institute for Computing, Jülich,
NIC Series, Vol. **9**, ISBN 3-00-009055-X, pp. 259-269, 2002.

http://www.fz-juelich.de/nic-series/volume9

Exact Diagonalization Results for Strongly Correlated Electron-Phonon Systems

Holger Fehske[1], **Alexander Weiße**[1], **and Gerhard Wellein**[2]

[1] Physikalisches Institut, Universität Bayreuth, 95440 Bayreuth, Germany
E-mail: {holger.fehske, alexander.weisse}@uni-bayreuth.de

[2] Regionales Rechenzentrum Erlangen, Universität Erlangen, 91058 Erlangen, Germany
E-mail: gerhard.wellein@rrze.uni-erlangen.de

Combining Lanczos, density matrix, kernel polynomial moment and maximum entropy algorithms we study the ground-state and spectral properties of interacting electron-phonon systems on massively parallel and vector supercomputers. In order to illustrate the efficiency and reliability of our approach, we present numerical results for the single-polaron band dispersion, the Luttinger liquid to charge-density-wave metal insulator transition, and the interrelation of spin, charge, orbital and lattice degrees of freedom in colossal magnetoresistive manganites. The scalability and performance of our CRAY T3E-1200 implementation is briefly discussed.

1 Motivation and Projects

The role of coexisting electronic correlations and electron-lattice interactions is rapidly becoming central to determining many physical phenomena in important classes of novel materials, including the electronically quasi-one-dimensional (1D) organic polymers, halide-bridged metal chain complexes, and quantum spin (Peierls) systems, the quasi-2D high-T_c cuprate superconductors, as well as the 3D charge ordered nickelates and the colossal magnetoresistance manganites. From a theoretical point of view the challenge is to describe the partly exotic properties of these materials in terms of simplified microscopic models, taking into account the complex interplay of charge, spin, orbital and lattice degrees of freedom. Figure 1 gives a schematic survey of the physical problems and materials investigated in this context by the Bayreuth-Erlangen group at the John von Neumann Institute for Computing (NIC) during the last few years.

Adapting the corresponding model Hamiltonians to real physical situations one is frequently faced with the difficulty that the energy scales of electrons, phonons and their interaction are of the same order of magnitude, causing analytic methods to fail in most of these cases. Thus, at present, the most reliable results came from powerful numerical calculations like finite-cluster exact diagonalizations (ED), which are usually performed on supercomputers. As many other problems in theoretical physics, such ED studies are related to eigenvalue problems involving large sparse matrices. Iterative Lanczos or Jacobi-Davidson subspace methods are commonly used to determine the ground state and some excited eigenstates of the underlying Hamiltonian matrices. In general, the computational requirements of these eigenvalue algorithms are determined by a matrix-vector multiplication (MVM). MVM are also the most time and memory consuming step in the determination of spectral functions by kernel polynomial and maximum entropy methods. Thus the efficient use of modern supercomputers strongly depends on a parallel, fast and memory saving implementation of the MVM within the diagonalization routines. This was the main objective of our NIC project from the technical side.

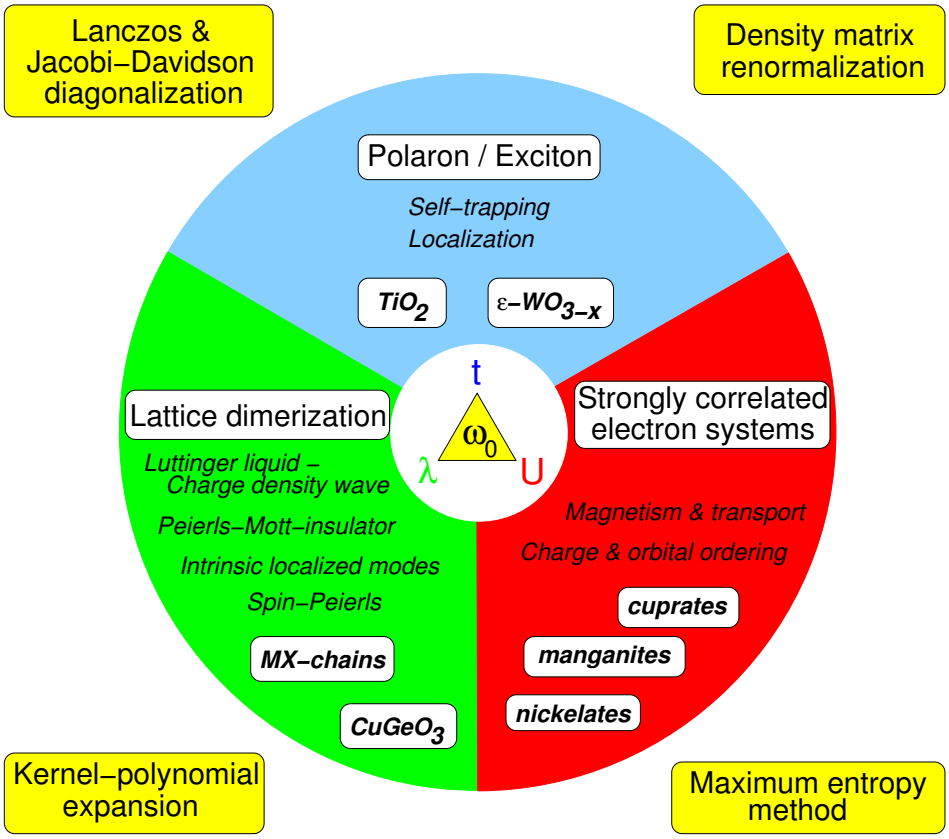

Figure 1. Summary of the NIC project. For more detailed information see the following original papers: (i) polaron/exciton problem[1], (ii) spontaneous dimerization transitions[2], (iii) polaronic effects in strongly correlated electron systems[3], and numerical methods[4].

2 Selected Physical Problems

2.1 Polaron Band Structure

The very fundamental problem of a single conduction electron coupled to the phonon degrees of freedom is still not completely understood. The challenge is to describe the crossover from a weakly (phonon) dressed charge carrier to a strongly mass-enhanced, less mobile polaronic quasiparticle with increasing electron-phonon (EP) coupling strength. This process is termed "self-trapping" since the distortion that tends to bind the carrier in a deformable lattice is induced by the particle itself, i.e., the trapping potential depends on the state of the carrier. Nonetheless, even if the quasiparticle is confined to a single lattice site (small polaron), this type of trapping does not imply localization of the electron. The tunneling between different lattice sites is still relevant and self-trapped states remain itinerant even though the coherent band motion is substantially reduced in the strong EP coupling limit.

Unfortunately, as yet none of the various analytical treatments, based, e.g., on perturbation expansions, are suitable for the investigation of the physically most interesting transition region, where the highly non-linear self-trapping process of the charge carrier takes place. That is because precisely in this situation the characteristic electronic and phononic energy scales are not well separated and non-adiabatic effects become increasingly important, implying a breakdown of the standard Migdal approximation.

We addressed the problem of polaron band formation in terms of the Holstein model by performing systematic Lanczos studies. The aim is to discuss the evolution of the quasiparticle band structure in dependence on the phonon frequency and EP interaction strength. The Holstein Hamiltonian reads:

$$\mathcal{H} = -t \sum_{\langle ij \rangle} (c_i^\dagger c_j + c_j^\dagger c_i) - g\omega_0 \sum_i (b_i^\dagger + b_i)(c_i^\dagger c_i - \tfrac{1}{2}) + \omega_0 \sum_i (b_i^\dagger b_i + \tfrac{1}{2}) \,, \qquad (1)$$

where $c_i^{[\dagger]}$ and $b_i^{[\dagger]}$ are the annihilation [creation] operators of (spinless) fermions and phonons at Wannier site i, respectively. In (1), the following idealizations of real electron-phonon systems are made: (i) the electron transfer t is restricted to nearest-neighbour

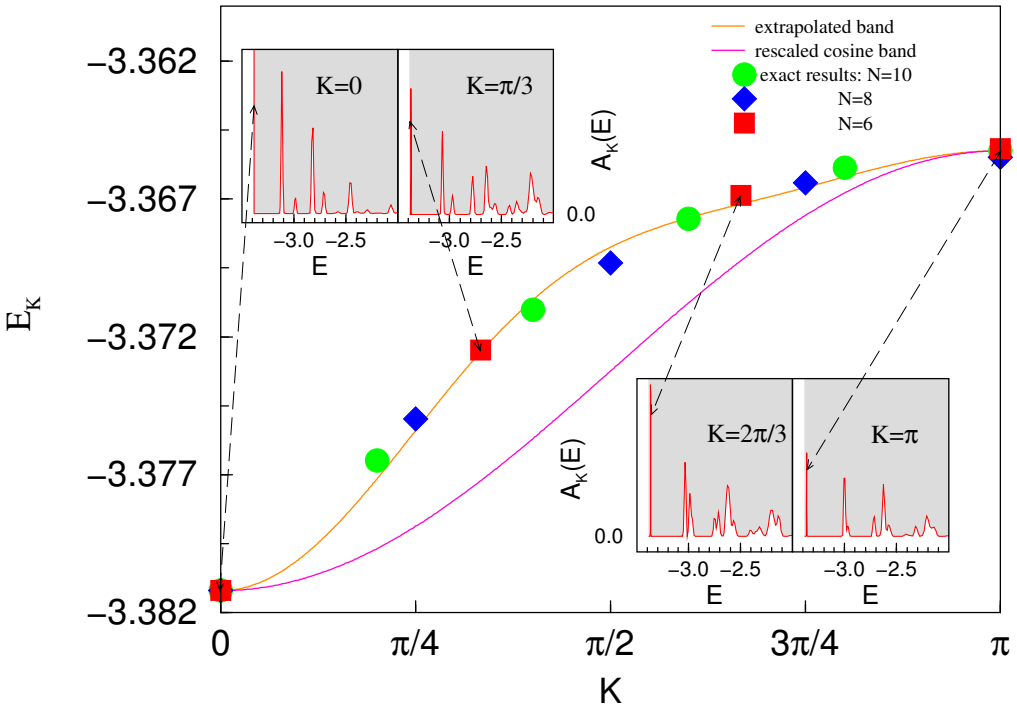

Figure 2. Band dispersion $E(K)$ of a single electron described by the Holstein model on 1D rings with N sites, where $g = 2.73$ and $\omega_0 = 0.4$. The insets show the low-energy part of the one-particle spectral function A_K(E) for selected momenta K. The magenta line corresponds to the dispersion of a free particle with a renormalized bandwidth. The orange line gives a least-squares fit to an effective band dispersion $\tilde{E}_K = \sum_{l=0}^{3} a_l \cos lK$.

pairs $\langle ij \rangle$; (ii) the charge carrier is locally coupled to a dispersionsless optical phonon mode (g denotes the EP coupling constant and ω_0 is the bare phonon frequency); (iii) the phonons are treated within a harmonic approximation.

In order to determine the polaron band structure, at first one has to calculate the wave-vector resolved spectral density function $A_{\vec{K}}(E) = \sum_n |\langle \Psi^{(1)}_{n,\vec{K}} \,|\, c^\dagger_{\vec{K}} \,|\, 0 \rangle|^2 \, \delta(E - E^{(1)}_n)$. Then the so-called "coherent" band dispersion, $E_{\vec{K}}$, can be extracted from the first peak of $A_{\vec{K}}(E)$ having finite spectral weight ($|\Psi^{(1)}_{n,\vec{K}}\rangle$ is n-th excited state in a certain $\vec{K}$-sector).

Figure 2 displays a typical polaron band dispersion obtained for the crossover regime. $E_{\vec{K}}$ exhibits several striking features: (i) Although we observe all signs of the famous polaronic band collapse, at intermediate-to-strong EP couplings the coherent bandwidth is by about a factor of 3 times larger than predicted by the standard Lang-Firsov formula $\Delta E_{LF} = 4t \exp[-g^2]$. (ii) The effective polaronic band dispersion deviates substantially from a simple tight-binding cosine band due to further than nearest-neighbour ranged hopping processes induced by the residual polaron-phonon interaction. As a consequence, the polaronic mass enhancement is substantially weakened. (iii) The flattening of the band dispersion at large momenta, which is normally observed in the weak-coupling case, persists to surprisingly large interaction strengths, even if the renormalized band width is by one order of magnitude smaller than the bare phonon frequency.

2.2 Luttinger-Liquid vs. Charge-Density-Wave Behaviour

Low dimensional electronic materials are known to be very susceptible to structural distortions driven by the EP interaction. Probably the most famous one is the Peierls instability of 1D metals: As the temperature is lowered the system creates a periodic variation in charge density, called a "charge-density-wave" (CDW), by shifting the electrons and ions from their symmetric positions. For the half-filled band case the dimerization of the lattice opens a gap at the Fermi surface; as a result the metal is transformed into an insulator.

Most theoretical treatments of the Peierls instability describe the lattice degrees of freedom classically. In a wide range of quasi-1D metals, however, the lattice zero-point motion is comparable to the Peierls lattice distortion, which makes the rigid lattice approximation questionable. By any means lattice dynamical (quantum phonon) effects should be included in the theoretical analysis of transport and optical phenomena.

Let us consider the 1D Holstein model of spinless fermions, Eq. (1), at half-filling ($N_e = N/2$). This model is of physical relevance in the strong interaction limit of the Hubbard model ($U \to \infty$). Based on a density-matrix algorithm for the phonon Hilbert space reduction, we have diagonalized the Holstein model on chains of even length with up to 12 sites using periodic boundary conditions. The resulting phase diagram is shown in Fig. 3. For small g quantum phonon fluctuations destroy the dimerized ground state and the system becomes a metal, more precisely a Luttinger liquid LL, with parameters that vary with the coupling. For large g the system has an energy gap and develops true long-range CDW order in the thermodynamic limit. The phase boundary obtained with our optimized phonon diagonalization methods was confirmed by the density matrix renormalization group (DMRG) results by Bursill *et al.* (Phys. Rev. Lett. **83**, 408 (1999)). In the adiabatic limit $\omega_0 = 0$, the critical coupling converges to zero. In the strong-coupling anti-adiabatic regime, the half-filled Holstein model can be transformed to the exactly soluble

XXZ model, which exhibits a Kosterlitz-Thouless phase transition (long-dashed curve in Fig. 3).

The LL and CDW phases can be characterized in more detail. According to Haldane's Luttinger liquid conjecture, 1D gapless systems of interacting fermions should belong to the same universality class as the Tomonaga-Luttinger model. As stated above, the Holstein system is gapless for small enough coupling g. The left insets of Fig. 3 give the LL parameters as a function of g in the region, where our Lanczos data obey the LL finite-size scaling relations, $\frac{E_0(N)}{N} = \epsilon_\infty - \frac{\pi u_\rho}{6N^2}$ and $E_{\pm 1}(N) - E_0(N) = \frac{\pi u_\rho}{2K_\rho N}$. Here ϵ_∞ ($E_0(N)$) denotes the ground-state energy per site of a infinite (finite) system (of N sites), K_ρ is the effective coupling (stiffness) constant, and u_ρ is the velocity of the charge excitations.

A very interesting result is that for small frequencies the effective fermion-fermion interaction is attractive, while it is repulsive for large frequencies, where the system forms a polaronic metal. Obviously there is a transition line in between, where the model de-

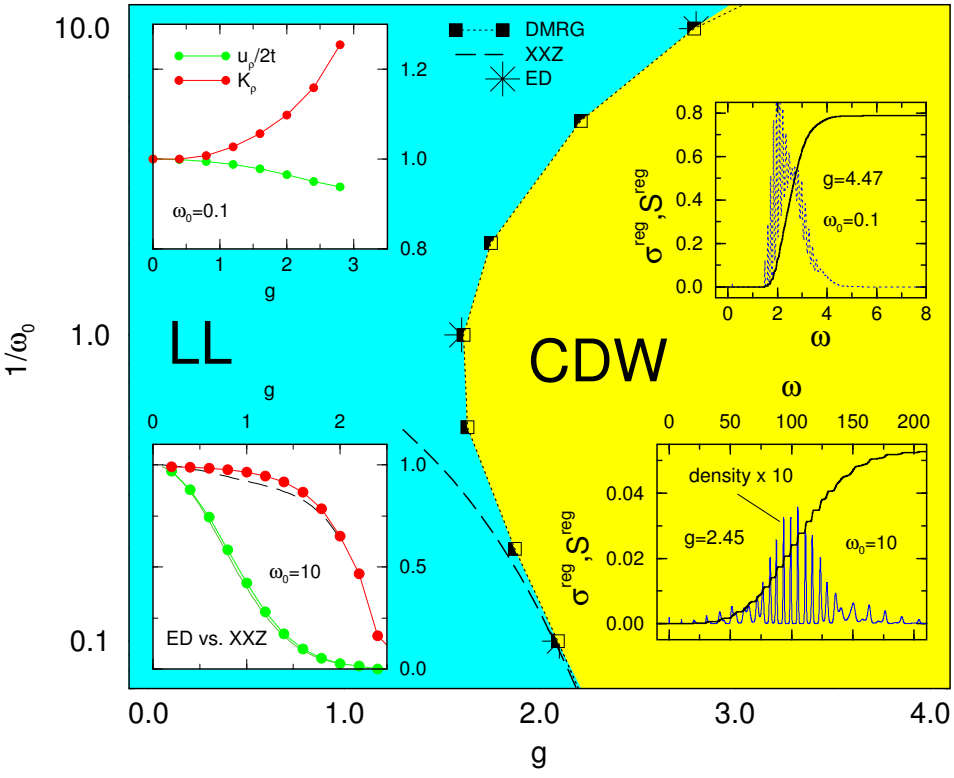

Figure 3. Ground-state phase diagram of the 1D Holstein model of spinless fermions at half-filling ($N_e = N/2$), showing the boundary between the Luttinger liquid (LL) and charge-density-wave (CDW) states obtained by ED and DMRG approaches. Left insets show the LL parameters u_ρ and K_ρ as a function of the electron-phonon coupling g in the metallic regime; right insets display for a six-site chain the regular part of the optical conductivity $\sigma^{reg}(\omega)$ (dotted lines) and the integrated spectral weight $\mathcal{S}^{reg}(\omega) = \int_0^\omega d\omega' \sigma^{reg}(\omega')$ (solid lines) in the CDW region.

scribes "free" particles in lowest order. In the CDW state valuable information about the low-energy excitations can be obtained from the optical conductivity, which can be evaluated by means of very efficient and numerically stable Chebyshev recursion and maximum entropy algorithms. The optical absorption spectrum in the strong EP coupling regime is quite different from that in the LL phase. It can be interpreted in terms of strong EP correlations and corroborates the CDW picture. In the adiabatic region (upper right inset), the broad optical absorption band is produced by a single-particle excitation accompanied by multi-phonon absorptions. The most striking feature is the large spectral weight contained in the incoherent part of optical conductivity. Employing the f-sum rule for the optical conductivity and taking into account the behaviour of the kinetic energy ($\propto u_\rho$) as function of g, we found that in the metallic LL and insulating CDW phases nearly all the spectral weight is contained in the coherent (Drude) and incoherent (regular) part of Re $\sigma(\omega)$, respectively.

2.3 Lattice Dynamical Effects in CMR Manganites

The transition from a metallic ferromagnetic low-temperature phase to an insulating paramagnetic high-temperature phase observed in some hole-doped manganese oxides (e.g. in $\mathrm{La_{1-x}[Sr,Ca]_xMnO_3}$) is associated with an unusual dramatic change in their elec-

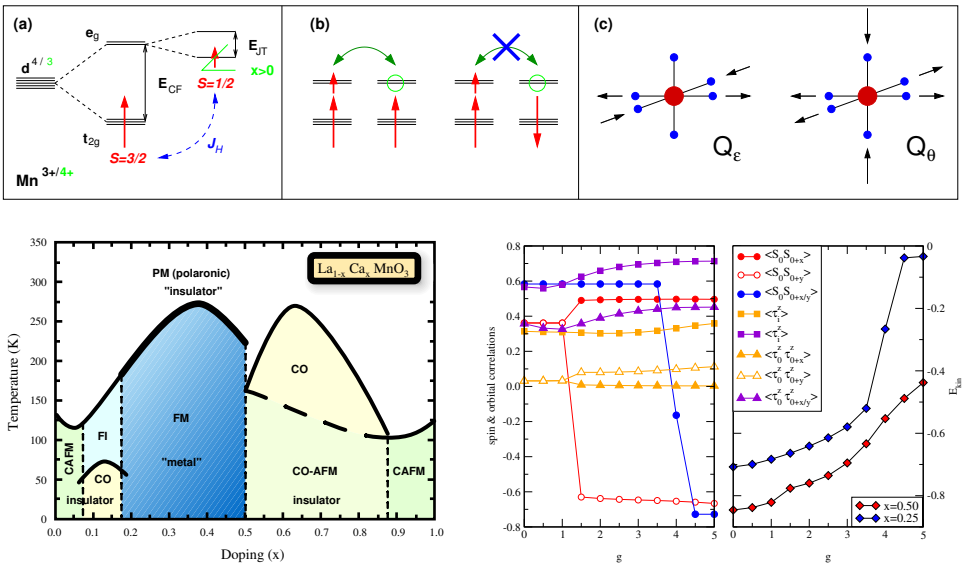

Figure 4. *Upper panel:* (a) Crystal-field and Jahn-Teller splitting of the five-fold degenerate atomic Mn 3d levels (half-filled t_{2g} triplets form local spins $S = 3/2$ interacting ferromagnetically with electrons in single occupied e_g levels); (b) double-exchange model (the hopping amplitude reaches is maximum if the core spins are aligned and vanishes in the case of antiparallel orientation) ; (c) Jahn-Teller modes. *Lower panel:* Schematic phase diagram of $\mathrm{La_{1-x}Ca_xMnO_3}$ reproduced from E. Dagotto *et al.* [Phys. Rep. **344** (2001)] (FM: Ferromagnetic Metal; FI: Ferromagnetic Insulator; AF: Antiferromagnet; CAF: Canted AF, and CO: Charge/Orbital Ordering (left figure)). Kinetic energy, selected spin and orbital correlation functions for the CMR model on a 4-site cluster, where $t_{(\mathrm{t_{2g}})} = 1/3$, $J_H = 1.75$, $U = 15$, and $\omega_0 = 0.0175$ in units of $t_{(\mathrm{e_{2g}})} = 0.4$ eV (right figures).

tronic and magnetic properties, including a spectacularly large negative magnetoresistive response to an applied magnetic field, which might have important technological applications.

Early studies on lanthanum manganites concentrated on the link between magnetic correlations and transport, and attributed the low-T metallic behavior to Zener's double-exchange mechanism , which maximizes the hopping of a strongly Hund's rule coupled Mn e_g-electron in a polarized background of the core spins (Mn t_{2g}-electrons) (see Fig. 4). Recently it has been argued that physics beyond double-exchange is important not only to explain the very complex phase diagram of the manganites but also the colossal magnetoresistance (CMR) transition itself. More specifically, orbital and lattice effects seem to be crucial in explaining the CMR phenomenon. There are two types of lattice distortions which are important in manganites. First the partially filled e_g states of the Mn^{3+} ion are Jahn-Teller active, i.e., the system can gain energy from a quadrupolar symmetric elongation of the oxygen octahedra which lifts the e_g degeneracy. A second possible deformation is an isotropic shrinking of a MnO_6 octahedron. This "breathing"-type distortion couples to changes in the e_g charge density, i.e., is always associated with the presence of an Mn^{4+} ion. In the heavily doped material, both, breathing-mode collapsed (Mn^{4+}) and Jahn-Teller distorted (Mn^{3+}) sites are created simultaneously when the holes are localized in passing the CMR metal insulator transition.

To investigate the interaction of charge, spin, orbital and lattice degrees of freedom in CMR manganites without uncontrolled approximations, we performed exact diagonalizations based on the following very general Hamiltonian

$$
\begin{aligned}
H &= H_{\text{double-exchange}} + H_{\text{electron-phonon}} + H^{\text{2nd order}}_{\text{spin-orbital}} + H_{\text{phonon}} \\
&= \sum_{i,\delta,\alpha,\beta} \left(a_{i,\uparrow} a^{\dagger}_{i+\delta,\uparrow} + a_{i,\downarrow} a^{\dagger}_{i+\delta,\downarrow}\right) t^{\delta}_{\alpha\beta}\, c^{\dagger}_{i,\alpha} n_{i,\bar{\alpha}} n_{i+\delta,\bar{\beta}} c_{i+\delta,\beta} \\
&\quad + g\omega_0 \sum_i \Big[(n_{i,\epsilon} - n_{i,\theta})(b^{\dagger}_{i,\theta} + b_{i,\theta}) + (c^{\dagger}_{i,\theta} c_{i,\epsilon} + c^{\dagger}_{i,\epsilon} c_{i,\theta})(b^{\dagger}_{i,\epsilon} + b_{i,\epsilon})\Big] \\
&\quad + \sum_{i,\delta,\xi,\zeta} \left(J^{\delta}_{\xi\zeta}\, \mathbf{S}_i \mathbf{S}_{i+\delta} + \Delta^{\delta}_{\xi\zeta}\right) P^{\xi}_i P^{\zeta}_{i+\delta} + \omega_0 \sum_i \Big[b^{\dagger}_{i,\theta} b_{i,\theta} + b^{\dagger}_{i,\epsilon} b_{i,\epsilon}\Big] \,, \qquad (2)
\end{aligned}
$$

containing Schwinger bosons $a^{(\dagger)}_{i,\mu}$, i.e. $\mathbf{S}_i = a^{\dagger}_{i,\mu} \boldsymbol{\sigma}_{\mu\nu} a_{i,\nu}$ ($\mu, \nu \in \{\uparrow, \downarrow\}$), fermionic holes $c^{(\dagger)}_{i,\alpha}$, phonons $b^{(\dagger)}_{i,\alpha}$ ($\alpha \in \{\theta, \epsilon\}$), and orbital projectors P^{ξ}_i.

Exemplarily, in Fig. 4 we show the dependence of nearest neighbour spin and orbital correlations and of the kinetic energy on the strength of the EP coupling g. For doping level $x = 0.25$, which corresponds to the metallic regime, we found pronounced ferromagnetic correlations of both actual spins ($\mathbf{S}$) and z-components of the pseudo-spins τ^z (representing orbitals, $\tau^z_i = n_{i,\theta} - n_{i,\epsilon}$). Only at very large EP couplings, a "trapping" of the e_g-electrons takes place (cf. the behaviour of E_{kin} in Fig. 4), accompanied by the development of strong antiferromagnetic spin correlations. In contrast, at $x = 0.5$, a transition from a "ferromagnetic state" to an "antiferromagnetic state" with weak ferromagnetic spin correlations in $x-$direction is observed for a relatively modest EP interaction ($g_c \simeq 1$). Note that in this "phase" spin and pseudospin ordering is anticorrelated, and the absolute value of the kinetic energy shows a rather smooth decrease with increasing g. Of course, to be more predictive, ED of larger systems would be highly desirable.

3 Numerical Concepts and Methods

In general, ED studies of microscopic electron-phonon models involve very large sparse matrices, even for small clusters. Thus both continuous access to the most powerful supercomputers and steady improvements of algorithms and implementations are the technical basics of our project. In the past years the algorithms listed below have been successfully implemented on numerous architectures including CRAY T3E, NEC SX-4/5, IBM SP, Fujitsu VPP700 and Hitachi SR8000 supercomputers.
In order to discuss a wide variety of physical quantities and ensure an efficient use of supercomputers at same time we use a wide variety of algorithms and techniques:

- Lanczos diagonalization:
  The standard Lanczos algorithm is employed to compute non-degenerate ground states . In that case the Lanczos algorithm provides rapid convergence and low memory consumption which allows us to determine ground states of matrices up to a dimension of $D_{\rm tot} \sim 4 \times 10^9$ on the CRAY T3E at NIC.

- Jacobi-Davidson algorithm with pre-conditioning:
  In a joint project with A. Basermann (NEC) a Jacobi-Davidson algorithm was implemented to compute eigenstates in the low-energy spectrum with high resolution (including degeneracies): In typical production jobs a maximum of 50 eigenvalues with matrix dimension of $D_{\rm tot} \sim 10^7$ can be computed at the same time.

- Kernel-polynomial expansion and maximum-entropy method
  A high quality approximation of spectral properties (involving all eigenstates) of large sparse matrices can be obtained using a Kernel-polynomial expansion in combination with a maximum-entropy method. This technique is applied to matrices up to a dimension of $D_{\rm tot} \sim 4 \times 10^9$ and provides results which can be compared qualitatively with experimental data.

- Density-matrix algorithm:
  In selected parameter regions the matrix dimension can be substantially reduced by a transformation from bare phonon states to optimal phonon states. This transformation can be determined by a density-matrix algorithm in combination with a sequence of several hundred Lanczos diagonalization steps involving the matrix with reduced dimension.

The memory requirement and compute time of all algorithms is determined by a MVM step involving the large sparse matrix. Of course symmetries and conservation laws are exploited to reduce the matrix dimension. Nonetheless the matrix dimension and the quality of our calculations is mainly limited by the available memory. Therefore the large amount of memory per node on CRAY T3E-1200 at NIC has been a valuable benefit for our project. With regard to the coding of the MVM step two supplementary strategies have been chosen. The *in core* implementation stores the non-zero matrix-elements only, using storage techniques like the *compressed row storage* format or the *jagged diagonals storage* format. Together with a parallel MVM implementation based on non-blocking `MPI` (message passing interface) communication calls, the in core version provides high scalability and numerical performance at the cost of additional memory consumption. On the contrary, the

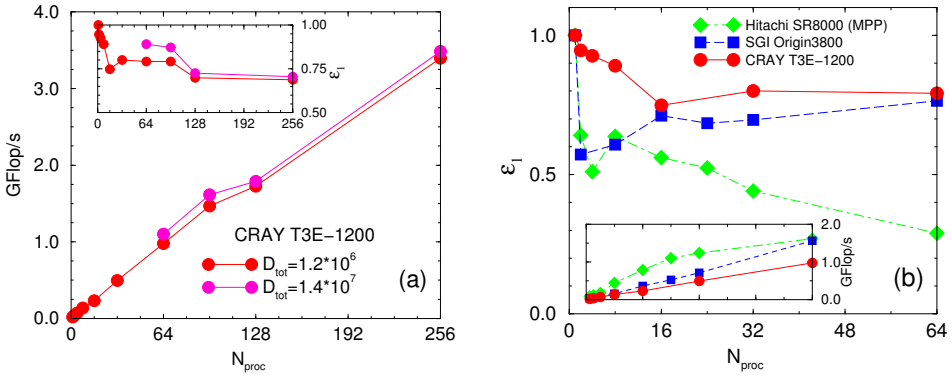

Figure 5. Performance of MVM step on CRAY T3E-1200 for different matrix sizes (a) and parallel efficiency at fixed matrix size for different supercomputers (b). The insets show the corresponding parallel efficiencies ϵ_1 (a) and total performance numbers (b). Due to the memory requirements a minimum processor number of 64 had to be used for $D_{tot} = 1.4 \times 10^7$ and the corresponding parallel efficiency has been scaled to the single processor performance of $D_{tot} = 1.2 \times 10^6$. Note: In (b) the Hitachi SR8000-F1 has been used in the massively parallel (MPP) mode and the SGI Origin3800 has been equipped with MIPS R12000-500 MHz processors.

out core implementation does not even store the non-zero matrix-elements but recomputes the entries in each MVM step. In combination with algorithms (1) and (3) this technique allows us to reach very high matrix dimensions at the cost of additional computational effort. To optimize the scalability of the out core version a lot of work has been done to preserve the natural parallelism (direct product of electron and phonon Hilbert spaces) in the parallel program even for symmetrized basis states. Furthermore we have developed both a portable MVM based on non-blocking `MPI` communication calls and a CRAY specific version using the `shmem` library.
The single processor performance of the algorithms used is clearly limited by the available memory-bandwidth, because the sparse MVM step does not allow major cache-reuse. However, the total performance of the parallel implementation strongly depends on a well balanced ratio between local and remote memory bandwidth.

4 Performance Analysis on Supercomputers

The CRAY T3E series is widely regarded as a paradigm for scalability. Thus the efficient use of these systems is closely connected with the ability of algorithms and programs to scale to hundreds of processors. We have chosen an exemplary benchmark for our in core MVM implementation to deliver insight in the average performance characteristics of our computations. As a measure of scalability we use the parallel efficiency

$$\epsilon_1(N_{proc}) = T(1)/(N_{proc} \times T(N_{proc})) \tag{3}$$

[$T(N_{proc})$ is the time per MVM step on N_{proc} processors] at fixed problem size (Fig. 5).

For small to intermediate processor numbers (up to 96) a parallel efficiency of more than 75% can be sustained. Although there is a drop in the efficiency at 128 processors, our MVM implementation provides a scalable algorithm because it still exceeds an efficiency

of 70% even for 256 processors and there is only a minor performance dependence on the problem size. Most notably, the CRAY T3E provides outstanding scalability even when compared with next generation supercomputers as can be seen from Fig. 5 (b).

5 Concluding Remarks

The work presented in this report is an example for a successful interdisciplinary cooperation, spanning the fields of physics, algorithmic design and programming techniques. From the numerical point of view the overall goal was to develop valuable tools to perform fast and reliable many-body calculations on modern supercomputers. The implementation of the various optimized program packages on the T3E supercomputer at the NIC provided new and exciting insights to the interaction of electronic and phononic degrees of freedom in the currently most intensive studied novel materials: the quasi-1D metals and charge-density-wave systems, high-T_c cuprates, polaronic nickelates and CMR manganites.

Acknowledgements

We are particularly indebted to the NIC Jülich, LRZ München and HLR Stuttgart for the generous granting of their parallel computer facilities. We acknowledge useful discussions with N. Attig, A. Basermann, E. Jeckelmann, B. Steffen, and R. Vogelsang.

References

1. H. Fehske, J. Loos and G. Wellein, *Spectral properties of the 2D Holstein polaron*, Z. Phys. B **104**, 619 (1997);
   G. Wellein and H. Fehske, *Polaron band formation in the Holstein model*, Phys. Rev. B **55**, 4513 (1997);
   G. Wellein and H. Fehske, *On the self-trapping problem of electrons or excitons in one dimension*, Phys. Rev. B **58**, 6208 (1998);
   H. Fehske, J. Loos, and G. Wellein, *Lattice polaron formation: Effects of non-screened electron-phonon interaction*, Phys. Rev. B **61**, 8016 (2000);
   F.-X. Bronold and H. Fehske, *Anderson localization of polaron states*, arXiv:cond-mat/0110528.
2. A. Weiße and H. Fehske, *Peierls instability and optical response in the one-dimensional half-filled Holstein model of spinless fermions*, Phys. Rev. B, **58**, 13526 (1998);
   G. Wellein, H. Fehske, and A. P. Kampf, *Peierls dimerization with non-adiabatic spin-phonon coupling*, Phys. Rev. Lett. **81**, 3956 (1998);
   B. Büchner, H. Fehske, A. P. Kampf, and G. Wellein, *Lattice dimerization for the spin-Peierls compound $CuGeO_3$*, Physica B **259-261**, 956 (1999);
   A. Weiße, G. Wellein, and H. Fehske, *Quantum lattice fluctuations in a frustrated Heisenberg spin-Peierls chain*, Phys. Rev. B **60**, 6566 (1999);
   H. Fehske, M. Holicki, and A. Weiße, *Lattice dynamical effects on the Peierls transition in one-dimensional metals and spin chains*, Advances in Solid State Physics **40**, 235 (2000);

H. Fehske, M. Kinateder, G. Wellein, and A. R. Bishop, *Quantum lattice effects in mixed-valence transition-metal chain complexes*, Phys. Rev. B **63**, 245121 (2001);
H. Fehske, G. Wellein, A. Weiße, F. Göhmann, H. Büttner, and A. R. Bishop, *Peierls-insulator Mott-insulator transition in 1D*, arXiv:cond-mat/0106116, Physica B **312-313**,562-563 (2002).

3. G. Wellein, H. Fehske, H. Büttner, and A. R. Bishop, *On the stability of polaronic superlattices in strongly coupled electron-phonon systems* Proc. Int. Conf. M^2S HTSC V, Beijing China, 1997, Physica C **282-287**, 1827 (1997);
B. Bäuml, G. Wellein, and H. Fehske, *Optical absorption and single-particle excitations in the 2D Holstein t-J model*, Phys. Rev. B **58**, 3663 (1998);
H. Fehske, G. Wellein, and H. Büttner, *Pairing susceptibility of strongly correlated electrons weakly coupled to the lattice*, J. Supercond., **12**, 65 (1999);
A. Weiße, J. Loos, and H. Fehske, *Two-phase scenario for the metal-insulator transition in CMR manganites*, Phys. Rev. B **64**, 104413 (2001).
4. G. Wellein and H. Fehske, *Towards the limits of present-day supercomputers: Exact diagonalization of strongly correlated electron-phonon systems* in *High Performance Computing in Science and Engineering '99* edited by E. Krause and W. Jäger, Springer-Verlag Berlin Heidelberg (2000), pp 112-129;
M. Kinateder, G. Wellein, A. Basermann, and H. Fehske, *Jacobi-Davidson algorithm with fast matrix vector multiplication on massively parallel and vector supercomputers*, in *High Performance Computing in Science and Engineering '00* edited by E. Krause and W. Jäger, Springer-Verlag, Heidelberg (2001), pp 188-204;
A. Weiße, H. Fehske, G. Wellein, and A. R. Bishop, *Optimized phonon approach for the diagonalization of electron-phonon problems*, Phys. Rev. B **62**, R747 (2000);
G. Wellein, G. Hager, A. Basermann, and H. Fehske, *Exact Diagonalization of Large Sparse Matrices: A Challenge for Modern Supercomputers*, CD CUC, Indian Wells, USA, April 2001;
A. Weiße, G. Wellein, and H. Fehske, *Density-matrix algorithm for phonon Hilbert space reduction in the numerical diagonalization of quantum many-body systems*, in *High Performance Computing in Science and Engineering '01* edited by E. Krause and W. Jäger, Springer-Verlag, Heidelberg (2002), pp 131-144.